JBC ARTICLE

Discovery of a heme-binding domain in a neuronal voltage-gated potassium channel

Mark J. Burton[1,2,‡], Joel Cresser-Brown[3,‡], Morgan Thomas[1,2], Nicola Portolano[1,2], Jaswir Basran[2,4], Samuel L. Freeman[3], Hanna Kwon[3], Andrew R. Bottrill[5], Manuel J. Llansola-Portoles[6], Andrew A. Pascal[6], Rebekah Jukes-Jones[7], Tatyana Chernova[7], Ralf Schmid[2,4], Noel W. Davies[2,4], Nina M. Storey[2,4], Pierre Dorlet[8], Peter C. E. Moody[4], John S. Mitcheson[4], and Emma L. Raven[3,*]

From the Departments of [1]Chemistry and [4]Molecular and Cell Biology, the [2]Leicester Institute of Structural and Chemical Biology, and the [5]Protein Nucleic Acid Chemistry Laboratory, University of Leicester, Leicester, United Kingdom, the [3]School of Chemistry, University of Bristol, Bristol, United Kingdom, the [6]Université Paris-Saclay, CEA, CNRS, Institute for Integrative Biology of the Cell, Gif-sur-Yvette, France, the [7]Medical Research Council Toxicology Unit, University of Cambridge, Leicester, United Kingdom, and [8]CNRS, Aix Marseille Université, Laboratoire de Bioenergetique et d'Ingenierie des Protéines, Marseille, France

Edited by Michael J. Shipston

The EAG (*ether-à-go-go*) family of voltage-gated K$^+$ channels are important regulators of neuronal and cardiac action potential firing (excitability) and have major roles in human diseases such as epilepsy, schizophrenia, cancer, and sudden cardiac death. A defining feature of EAG (Kv10–12) channels is a highly conserved domain on the N terminus, known as the eag domain, consisting of a Per–ARNT–Sim (PAS) domain capped by a short sequence containing an amphipathic helix (Cap domain). The PAS and Cap domains are both vital for the normal function of EAG channels. Using heme-affinity pulldown assays and proteomics of lysates from primary cortical neurons, we identified that an EAG channel, hERG3 (Kv11.3), binds to heme. In whole-cell electrophysiology experiments, we identified that heme inhibits hERG3 channel activity. In addition, we expressed the Cap and PAS domain of hERG3 in *Escherichia coli* and, using spectroscopy and kinetics, identified the PAS domain as the location for heme binding. The results identify heme as a regulator of hERG3 channel activity. These observations are discussed in the context of the emerging role for heme as a regulator of ion channel activity in cells.

Per–ARNT–Sim (PAS) domains, first identified by sequence homology in the *Drosophila* proteins *period* and *single-minded*, and the vertebrate aryl hydrocarbon receptor nuclear transporter (ARNT), are well-known sensory modules present in a variety of signaling proteins in organisms ranging from bacteria to humans (1–3). PAS domains demonstrate considerable plasticity in binding different biologically relevant ligands. Relevant in the context of this work is their ability to bind heme as a ligand. The ligand-binding event is significant because it can act as a primary trigger to initiate a cellular signaling/regulatory response, or it can provide the PAS domain with a capacity to respond to secondary physical or chemical signals (such as binding of gas molecules, changes in redox potential, or light activation). In the case of heme as a ligand, there are several examples of heme-binding PAS domains that act as biological regulators in cells, for example the O$_2$ sensor proteins (*e.g.* FixL, *Escherichia coli* DOS) and the transcriptional regulators involved in circadian control (*e.g.* nPAS2, CLOCK, Rev-ERB, Per) (4, 5).

Several layers of regulatory control can be envisaged in the process of heme binding to a PAS domain protein. Heme binding might, for example, induce a conformational change in the PAS domain, which affects the interactions with partner proteins, and there is evidence for this in the heme-binding circadian proteins (6). Because known cell-signaling gases such as CO, NO, and O$_2$ all bind to heme (and with different affinities), the formation of a heme-bound PAS domain opens opportunities for the molecule to also respond to changes in concentrations of any or all of these cell-signaling gases. Thinking in these terms, it may not be a coincidence that CO and NO production in cells is catalyzed by two heme-containing proteins, heme oxygenase and nitric oxide synthase, respectively, both of which are themselves O$_2$-dependent. This interplay of heme- and gas-responsive PAS domains could provide the cell with highly versatile mechanisms for regulatory control that are at the same time responsive to changing concentrations of heme, O$_2$, CO, or NO. How these mechanisms play out has yet to be fully established.

In this paper, we present evidence from electrophysiological experiments for heme-dependent modulation of hERG3 (human *ether-à-go-go*–related gene 3, alternatively known as Kv11.3). We identify an interaction of heme with a PAS domain contained within the channel. Our results provide insight on the role of heme in channel regulation; we use this to discuss how heme-induced structural changes might be used to control channel function.

Results

Proteomics analyses

We sought to identify potential heme-binding proteins in neuronal lysates from primary cortical neurons, using heme-affinity chromatography and MS. Using this approach, we identified a number of proteins known to bind heme (*e.g.* mitochondrial enzymes), as well as proteins with unknown heme affinity; this included hERG3 (Fig. S1). In the structure of the overall
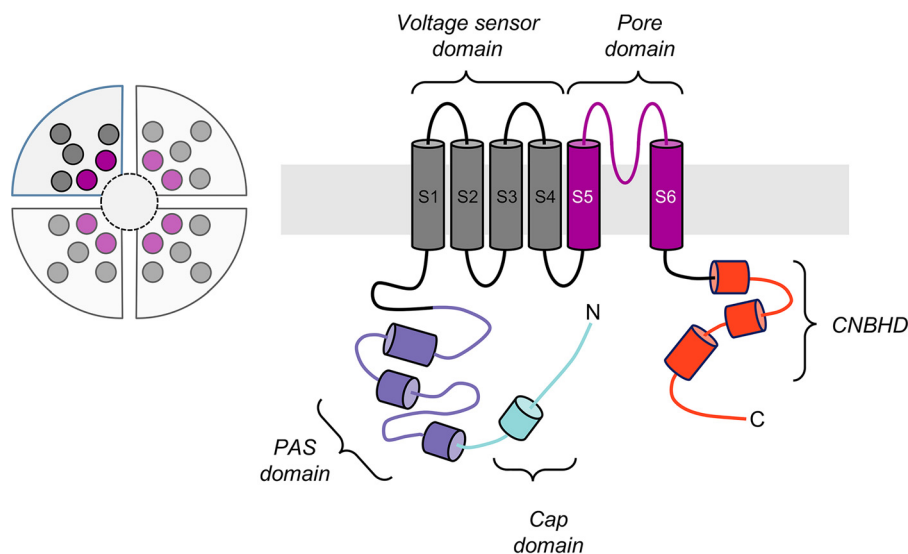
Figure 1. Schematic of the hERG3 channel subunit. *Left side*, hERG, which is part of the EAG family of ion channels, has four subunits, each shown as a quadrant, that assemble to form a tetrameric structure as shown in the circular schematic on the left. *Right side*, each subunit contains a transmembrane region, as well as cytoplasmic N- and C-terminal regions. The transmembrane region contains voltage sensor (helices S1–S4, *dark gray*) and pore-forming (helices S5 and S6, *magenta*) domains inside the membrane bilayer. The C-terminal cytoplasmic region contains a cyclic nucleotide-binding homology domain (*CNBHD, red*), which is connected to the transmembrane region via a structured domain usually referred to as the C-linker. The N-terminal cytoplasmic region (~400 residues) contains a region that is known as the eag domain (residues 1–135), which itself comprises a Cap domain (residues 1–26, *light blue*) and a PAS domain (residues 27–135, *purple*). This eag domain fragment (residues 1–135) has been expressed in this work and is referred to as hERG3-eag in this paper.

hERG3 channel, there are four subunits, each containing a transmembrane region, as well as cytoplasmic N- and C-terminal regions (Fig. 1) (7). The N-terminal cytoplasmic region (~400 residues) contains a highly conserved eag domain (residues 1–135), which itself comprises a Cap domain (residues 1–25) and a Per–ARNT–Sim (PAS) domain (residues 26–135).

Heme binding to the hERG3-eag domain

We expressed the Cap domain (residues 1–26) and the PAS (residues 27–135) domain of the hERG3 protein as an N-terminal His_6/S-tagged fusion protein in *E. coli* (Fig. 1 and Fig. S2); we will refer to this protein as hERG3-eag. Upon addition of heme to hERG3-eag, Fig. 2*A*, a species with Soret bands at 420 and 370 nm is observed, which we assign as arising from six- and five-coordinated heme, respectively. There is also a broad absorption envelope at 500–600 nm and a ligand-to-metal charge transfer band at 650 nm (Fig. 2*A*). These bands are similar to those reported for heme bound to proteins through Cys, Cys/His, or Cys/Xaa coordination (Table S1) (8). The presence of two bands in the Soret region is indicative of heterogeneity, which may arise either from changes in axial ligands or from different orientations of the bound heme (8–10). The ligands to the heme in hERG3 were not identified. The affinity of ferric heme for hERG3-eag was determined by titration ($K_d = 7.02 \pm 0.35$ μM; Fig. 2*A*, *inset, top panel*). Heme affinity can also be extracted from the first-order rate constant for transfer of heme to apo-myoglobin (which has a very high affinity for heme (11)); we measured this rate constant as $k_{off} = 0.03$ s^{-1} (Fig. 2*A*, *inset, bottom panel*), which is several orders of magnitude higher than for the globins and more in the range observed for other regulatory heme proteins (12).

Spectroscopic analysis of heme binding

Resonance Raman spectroscopy was used to provide more quantitative insight into the interaction of hERG3-eag with heme. In the high-frequency region, the spectrum of free heme displays the distinctive features of a ferric five-coordinate high-spin complex (5c-HS), with characteristic bands at 1372 (v_4), 1490 (v_3), and 1570 cm^{-1} (v_2) (Fig. 2*B*, *panel (i)*). The v_{10} mode of the 5c-HS species is hidden by the vinyl stretching bands expected in the 1610–1640-cm^{-1} region (1618 cm^{-1} for the in-plane and 1628 cm^{-1} for the out-of-plane vinyl group (13)). The ferric hERG3-eag–heme complex shows significant differences from free heme (Fig. 2*B*, *panel (ii)*). All the modes described for 5c-HS are present for the hERG3-eag–heme complex. Additionally, we observe bands at 1502 (v_3), 1553 and 1585 cm^{-1} (v_2), and 1640 cm^{-1} (v_{10}). These modes indicate the presence of a six-coordinate low-spin complex (Table S1) (14). These resonance Raman data are in agreement with the absorption spectra above and demonstrate the formation of a six-coordinated heme species with a specific binding environment.

EPR analyses support these conclusions, because the spectrum of the hERG3-eag–heme complex shows the formation of a low-spin heme complex (Fig. 2*C*). The spectrum is indicative of a mixture of species and was best simulated with two components (Fig. 2*C*). The g values for both are in good agreement with those of other ferric heme proteins bearing cysteine coordinated opposite a neutral sixth ligand (8). A Cys/His ligation is favored for both components as suggested by the placement in the Blumberg–Peisach diagram (Fig. 2*C*).

CO binds tightly ($K_d = 1.03 \pm 0.37$ μM; Fig. 3*A*) to the ferrous hERG3-eag–heme complex and gives a species (Soret band at 420 nm; Q-bands at 540 and 569 nm) that is characteristic of a normal CO-bound heme species. An identical species (Soret
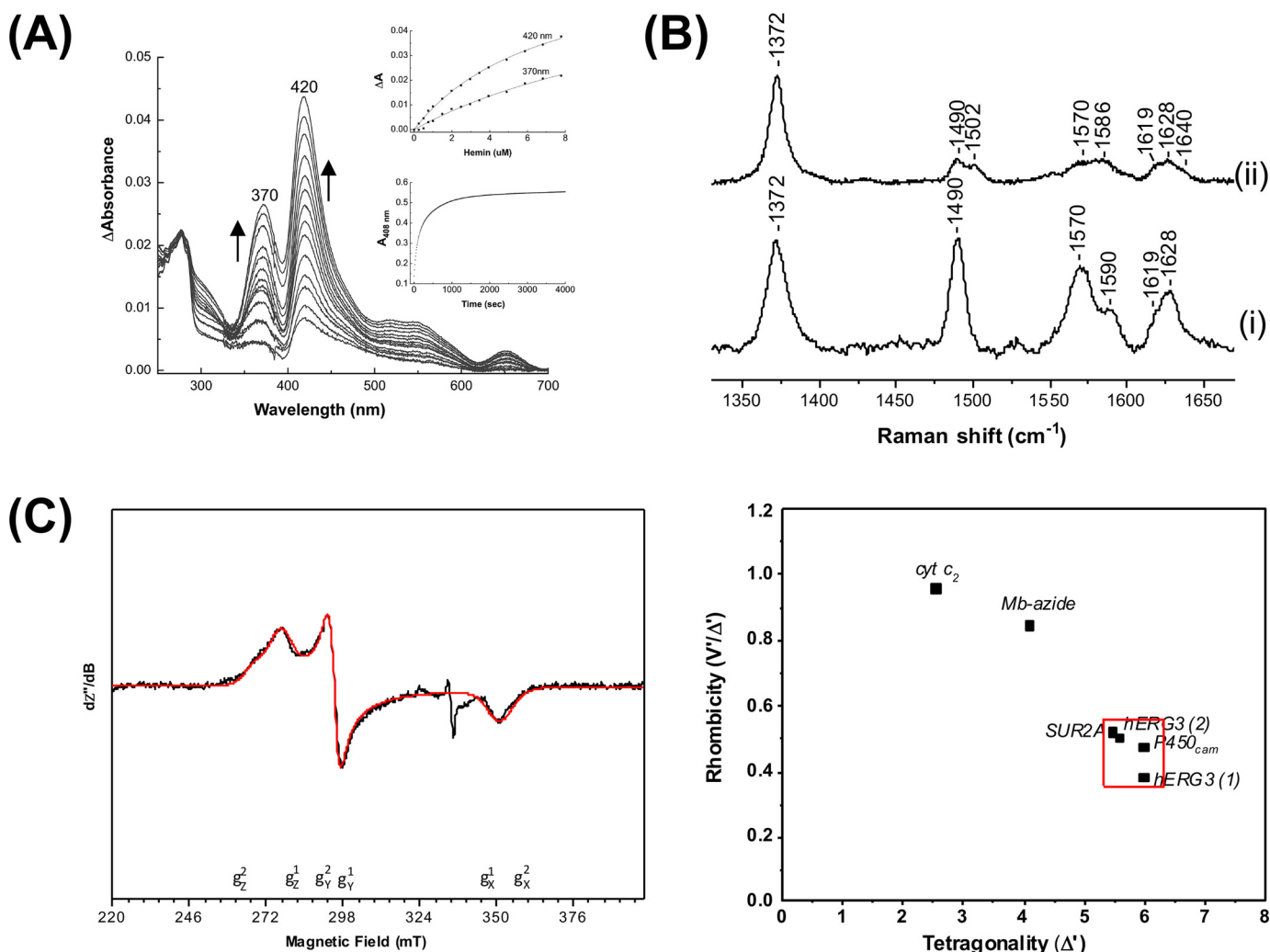
Figure 2. Analysis of heme binding to the hERG3-eag domain. *A*, difference spectra obtained on titration of the hERG3-eag domain with ferric heme; the *arrows* represent the directions of the absorbance changed with increasing heme concentration. *Inset, top panel*, hyperbolic fitting of the heme-binding data at both wavelength maxima to a 1:1 model for heme binding. *Inset, bottom panel*; absorbance changes at 408 nm on binding of the ferric hERG3-eag complex to apo-myoglobin. The data were fitted to the first order decay process, yielding $k_{obs} = 0.03$ s^{-1}. *B*, room temperature high-frequency resonance Raman spectra of free heme (*panel (i)*) and the ferric hERG3-eag–heme complex (*panel (ii)*). All spectra were collected with 413.1-nm laser excitation. *C, left panel*, X-band EPR spectrum (*black trace*) of the ferric hERG3-eag–heme complex in the low-spin region along with the simulated spectrum (*red trace*). The experimental conditions were as follows: microwave frequency, 9.38 GHz; microwave power, 0.064 mW; field modulation amplitude, 2 mT; field modulation frequency, 100 kHz; temperature, 15 K; [heme] = 100 μM, 5-fold excess of protein in 50 mM HEPES buffer, pH 7.5, 50 mM NaCl. The simulation parameters are as follows: species 1 (75%) *g* values (*g* strain) are $g_{z1} = 2.42$ (0.06), $g_{y1} = 2.27$ (0.00), and $g_{x1} = 1.91$ (0.04); species 2 (25%) *g* values (*g* strain) are $g_{z2} = 2.50$ (0,07), $g_{y2} = 2.28$ (0.00), and $g_{x2} = 1.90$ (0.06); Lorentzian linewidth full-width at half-maximum 4 mT. *Right panel*, Blumberg–Peisach correlation diagram showing EPR parameters plotted for various heme proteins.

band at 420 nm; Q-bands at 540 and 569 nm) is formed upon reaction of apo-hERG3-eag domain with a preformed heme–CO complex and with an affinity ($K_d = 10.55 \pm 1.34$ μM, data not shown) that is within reasonable range of the K_d for binding of CO to the ferrous hERG3-eag complex ($K_d = 1.03 \pm 0.37$ μM) as above. These spectra for the hERG3–heme–CO complex formed by two different routes are significantly different from that of a free heme–CO complex ($\lambda_{max} = 407$, 537, and 567 nm (12)), which indicates formation of a specific protein–heme–CO complex. The CO ligand is easily dissociated ($k_{off} = 0.03$ s^{-1}) in the presence of nitric oxide (Soret band at 390 nm; Fig. 3*B*), which is characteristic of a five-coordinated NO-bound heme protein complex (15, 16). These data indicate that the hERG3-eag–heme complex is competent for binding of biologically relevant gaseous ligands.

Structure of the hERG3-eag domain

The purified hERG3-eag protein was crystallized in the apo-form, in a monomeric state. The structure of the PAS domain (residues 18–135) is shown in Fig. 4*A* The hERG3-eag domain has a canonical PAS fold that comprises of five antiparallel β-sheets flanked by three α-helices, forming a hydrophobic cleft. This cleft is formed between the inner face of the β−sheet and the conformationally mobile F-helix. It is conserved in PAS domains known to bind ligands, including heme (3). The hERG3-eag structure contains a Cys[39]–Cys[64] disulfide bond (Fig. 4*A*) situated 12 residues from the F-helix and 13 residues from the Cap domain. The role of the disulfide bond is currently unknown and was not tested in this work, but it may impart a redox-sensing functionality to the PAS domain (as previously suggested (17–20)).
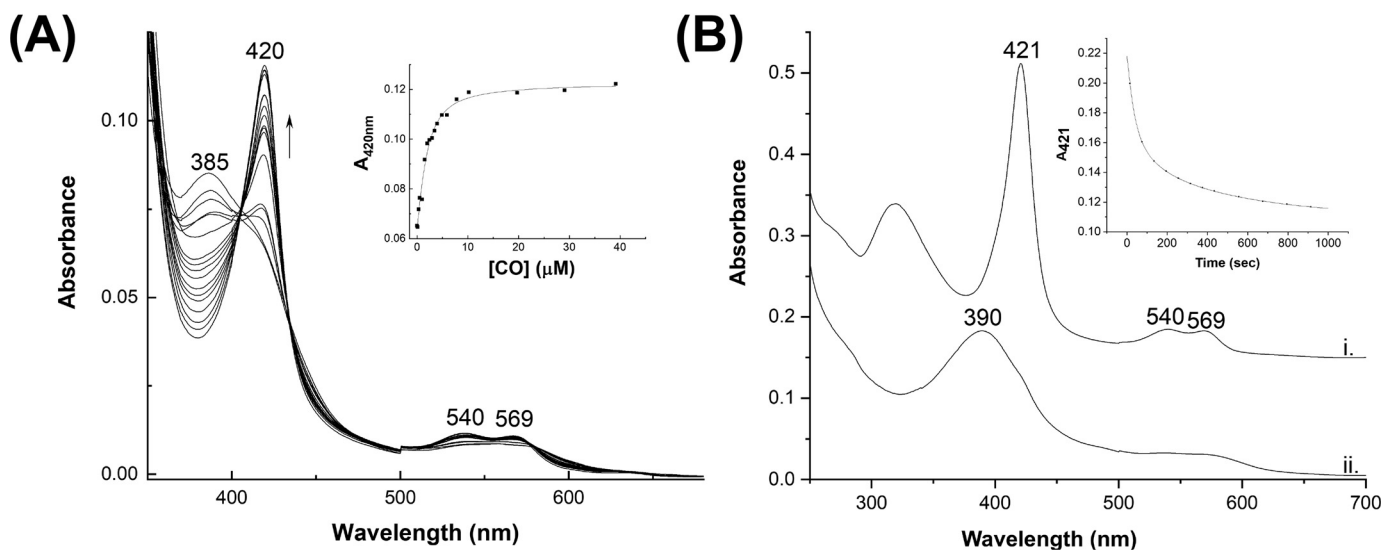
Figure 3. *A*, spectrophotometric titration of the ferrous hERG3-eag–heme complex with CO. *Inset*, quadratic (Morrison) fitting to the binding curve to give $K_d = 1.03 \pm 0.37$ μM. *B*, formation of a heme–NO–hERG3 complex ($\lambda_{max} = 390$ nm) on dissociation of CO from the ferrous heme–hERG3 complex (3 μM, $\lambda_{max} = 421$ nm) in the presence of NO. NO was formed from the NO releasing molecule, *S*-nitroso-*N*-acetyl penicillamine (see "Experimental procedures"). *Inset*, the 421-nm time course, fitted to a three-exponential process; using the dominant (50%) phase a rate constant for dissociation of CO, $k_{off(CO)}$, was determined ($k_{off(CO)} = 0.03$ s^{-1}).
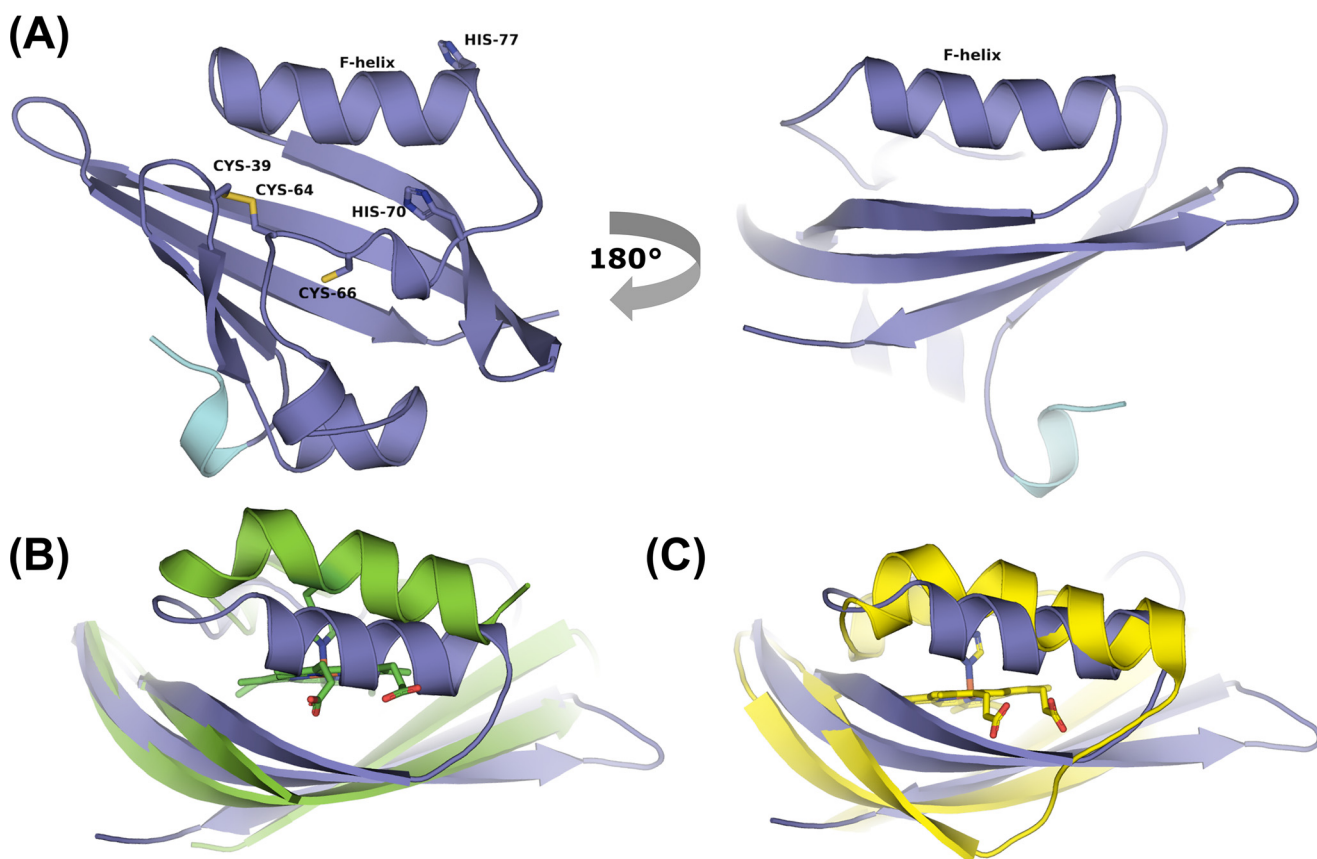

Figure 4. *A*, cartoon representation of the hERG3-eag crystal structure showing the PAS (*purple*) and Cap (*light blue*) domains; the color scheme used is the same as that used in Fig. 1 for the PAS and Cap domains. Potential heme-binding residues are labeled. *B* and *C*, structural alignment of hERG3-eag with structures of heme-bound PAS domains in *E. coli* DOS (Protein Data Bank code 1V9Y, *green* in *B*) and FixL (Protein Data Bank code 1DP6, *yellow* in *C*). Movement of the F-helix in *E. coli* DOS and FixL allows binding of the heme.

The first 17 residues at the N terminus are not seen in interpretable electron density in the crystal; furthermore, residues 18–23 are of weak density, indicating heterogeneity in this region (the N-terminal Cap). MS data (Fig. S2*C*) show there is a mixture of molecular weights with varying degrees of truncation at the N terminus (Fig. S2*D*), and the observed density

most likely reflects this mixture. Because a significant proportion of the protein is unaccounted for in the model, this probably explains the relatively high R values for a structure at this resolution (see Table S2). Despite attempts to obtain a co-crystal structure of heme-bound hERG3-eag, extensive co-crystallization and soaking experiments were unsuccessful. As we have noted previously (6), this does not mean that heme cannot bind to the protein, because the spectroscopic data clearly demonstrate that it does. It is more likely that the particular conformation selected for in the crystal structure is incompatible with heme binding, so that heme cannot bind to the protein during the crystallization process. Structural flexibility of the protein that is linked to the heme-binding event (see "Discussion") might also affect whether heme co-crystallizes with the protein.

Effect of heme on hERG3 channels

To measure the functional response of hERG3 channels to heme, hERG3 was heterologously expressed in Chinese hamster ovary cells. In whole-cell recordings, K^+ currents were elicited with the characteristic features of the hERG family (Fig. 5A), including slow voltage-dependent activation and deactivation, rapid onset, and recovery from inactivation and inhibition by astemizole (data not shown). Application of heme (Fig. 5, B–E) caused a substantial inhibition of hERG3 current at all potentials (shown here after >3 min). Mean ($\pm$ S.E.) heme inhibition of peak tail currents with a test potential to +40 mV was $63 \pm 12\%$ ($p < 0.05$, $n = 3$). Heme caused a small but significant negative shift in the voltage for half-maximal activation of 6.7 mV ($p < 0.05$, $n = 3$) (Fig. 5E). The lipophilic properties of heme and its ability to interact with membrane phospholipids allows it to be transported across the plasma membrane via passive diffusion (21). To test whether addition of intracellular heme also inhibited hERG3 channels, currents were recorded using the inside-out configuration of the patch clamp technique, and heme was applied directly to the cytoplasmic side of excised membrane patches. As reported with many other ionic currents, upon excision, a rapid decrease of hERG3 currents was observed in inside-out macropatches, consistent with loss of channel activity (rundown) upon removing the channels from the cellular environment. The addition of phosphatidylinositol 4,5-bisphosphate (10 μM) to the perfusate ameliorated rundown and resulted in stable recording conditions (Fig. 5, G and H). Subsequent application of heme (Fig. 5, F–H) to the intracellular side of the membrane caused inhibition of hERG3 currents in a similar manner as extracellularly applied heme in whole cell recordings. The time courses of heme inhibition were comparable, suggesting factors other than membrane diffusion of heme determine the rates of hERG3 current inhibition. These data demonstrate that heme inhibits hERG3 channel activity, thus connecting the heme-binding event to modulation of channel function.

Discussion

The EAG (Kv10–12) family of voltage-gated K^+ channels are regulators of neuronal and cardiac cell action potential firing (excitability). In humans, the family comprises hEAG, hERG, and hELK channels (22, 23). In this work, we have identified

heme-dependent regulation of hERG3 channel activity. Formation of a six-coordinated heme species is supported from resonance Raman data, as well as EPR and UV-visible spectra, and a heme-binding PAS domain within the eag domain of the channel has been identified.

Recent cryo-EM structural models of rat EAG1 and hERG1 confirm that the four eag domains are arranged around the periphery of the tetrameric intracellular assembly formed by the CNBHD and C-linkers (24, 25). The function of this large intracellular complex is to modulate voltage-dependent gating; profoundly influencing the time course and amplitudes of potassium currents during physiological processes such as action potentials. It sits underneath the transmembrane domains, with the C-linker connecting directly with the S6 activation gate. The PAS domain makes contacts predominantly with the CNBHD, whereas the Cap domain extends toward the interface between the voltage sensor, C-linker, and channel pore and thus is perfectly positioned to influence voltage- and time-dependent gating properties. Interestingly, functional studies reveal that deletion of the PAS and Cap domains has differential effects on the gating properties of hERG1 and hEAG1, suggesting that specific contacts with gating machinery of the two channels are different (26, 27). In hEAG1 channels, the eag domain is also required for calcium-calmodulin–dependent inhibition of current (26). hERG3 gating is similar to hERG1, and it is likely that the eag domain has a similar role in both channels, which is to slow deactivation gating and enhance inactivation gating.

PAS domains, which are known to bind heme (4, 5), have well-established roles in regulating the function of the related hERG1 channel (7, 28, 29), but heme binding to this channel has not been established. Heme has been shown to potently modulate the activity of a range of other potassium ion channels such as Kv1.4, large conductance Ca^{2+}-activated K channels, and ATP-activated K channels (12, 30–36). Our observation that heme binding reduces hERG3 activity furthers the notion that heme plays a deliberate modulatory role in these ion channel systems. As we noted in the introduction, the capacity for the heme group to also bind cell-signaling gases (CO, NO, O_2, or even H_2S) vastly broadens the range of stimuli that these ion channels could potentially be modulated by.

It is worth noting that heme is important for neuronal survival (37), and so a role for heme in the regulation of the "neuronal" channels hERG2 and hERG3 might reasonably be anticipated. At present, the biological basis for an interaction of heme with hERG3 is unknown, but a significant portion of brain damage caused during hemorrhagic stroke is believed to be due to the longer-lasting, cytotoxic effects of heme (38). More generally, an abundance of heme after traumatic events such as stroke and ischemia could conceivably disrupt the regulatory balance of ion channels in the brain and has cytotoxic implications for the cells involved (39). Heme-dependent inhibition of hERG3 would reduce repolarizing K^+ currents, potentially increasing neuronal excitability and susceptibility to cell death. An abundance of heme after traumatic events thus has the capacity to disrupt the dynamic processes surrounding the regulation of ion channel function if they are sensitive to heme.
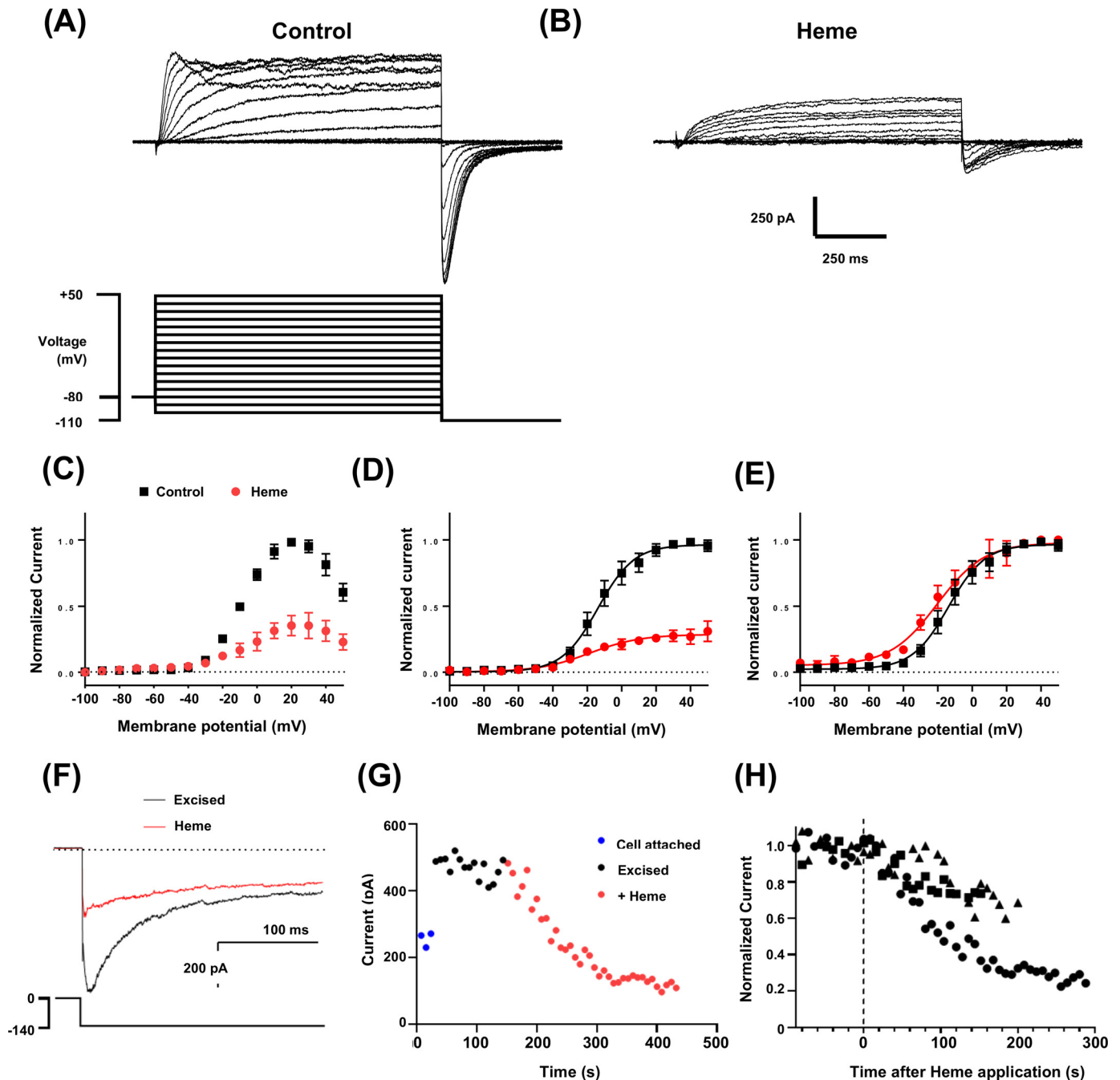
(A) Control

(B) Heme

250 pA

250 ms

Voltage (mV)

+50

−80

−110

(C)

■ Control ● Heme

Normalized Current

Membrane potential (mV)

(D)

Normalized current

Membrane potential (mV)

(E)

Normalized current

Membrane potential (mV)

(F)

— Excised
— Heme

100 ms

200 pA

0

−140

(G)

● Cell attached
● Excised
● + Heme

Current (pA)

Time (s)

(H)

Normalized Current

Time after Heme application (s)

Figure 5. hERG3 currents are inhibited by heme. *A*, representative whole-cell hERG3 currents (*upper panel*) elicited with voltage protocol (*lower panel*) consisting of 1-s test pulses from −100 to +50 mV in 10-mV increments and from a holding potential of −80 mV. Inward tail currents were measured at a potential of −110 mV. The start-start interval for the voltage protocol was 5 s. *B*, a family of hERG3 current traces from the same cell shown in *A* after superfusion of heme (500 nM). *C*, mean end-pulse current-voltage relationship with and without heme (500 nM) (*n* = 3). *D* and *E*, mean tail current (normalized to maximum control current in individual cells (*D*) or normalized to maximum current (*E*) in each recording solution) and plotted against test-pulse potential, with and without heme (500 nM) (*n* = 3). The data are fitted with Boltzmann functions (*solid lines*). Half-maximal activation ($V_{0.5}$) and slope factor were −12.3 ± 4.7 mV and 10.7 ± 1.0 mV, respectively, before heme and −19.0 ± 4.4 mV and 14.1 ± 2.6 mV with heme (*n* = 3). *F*, representative traces of excised inside-out macro-patch recordings of hERG3 tail currents before and during application of heme (1 μM). Patches were excised into solutions containing 10 μM phosphoinositol 4,5-bisphosphate to attenuate current rundown. Intracellular and extracellular solutions contained equimolar K⁺ concentrations. Tail currents were measured at a potential of −140 mV and following 2-s test pulses to 0 mV (see voltage protocol in *lower panel*). *Horizontal dotted lines* in *D–F* indicate zero current. *G*, representative plot of changes in amplitude of the deactivating component of the tail current plotted against time. The time between traces was 8 s. *H*, scatter plot of hERG3 tail current amplitudes in three separate excised patches plotted against time after heme application. The time of heme application is indicated by the *vertical dashed line*.

We did not identify the heme-binding location in hERG3-eag. However, we have compared the structure of apo-hERG3-eag with those of other heme-binding PAS domain proteins

(*Ec*DOS (40) and FixL (41)). Overlay of hERG3 with those of *Ec*DOS and FixL shows that, compared with the apo-hERG3 structure, there is a large movement of the F-helix in the heme-

bound *Ec*DOS and FixL structures to accommodate binding of the heme group (Fig. 4, *B* and *C*). It is feasible, therefore, that a similar mode of heme binding might occur in hERG3 if its F-helix is similarly flexible. Relevant in this context is the disulfide bond between Cys[39] and Cys[64], which is located 12 residues from the F-helix via a flexible loop. It has been proposed that disulfide bridges might serve as redox sensors in cells, by switching between thiol and disulfide structures (17–20). Loss of the Cys[39]–Cys[64] disulfide could facilitate movement of the F-helix, allowing heme to bind to the protein. The ligands to the bound heme are not identified as yet but candidate residues are His[70], His[77], and Cys[66] (Fig. 4*A*), which are in the vicinity of the proposed heme-binding site based on the comparison with *Ec*DOS and FixL. Cys/His axial ligations would be consistent with our spectroscopic data and with known ligations in other regulatory heme proteins (4, 5).

Based on our structure, we identify one further possible mechanism of heme-dependent regulation. The N-terminal Cap domain (residues 1–26) in hERG3-eag is mostly unresolved in our structure. In hERG1 the Cap domain, which contains a flexibly linked but stable amphipathic helix, is already known to affect channel activity (27, 42, 43). So in addition to affecting the conformation of the F-helix (as above), it is possible that heme binding to the PAS domain in hERG3 could also affect the orientation of the adjacent and potentially highly mobile Cap domain (Fig. 1). This N terminus is oriented toward the pore in the structure of the channel (25), and movements of the Cap domain might affect the conformations of the nearby cyclic nucleotide-binding homology domain, C-linker, voltage-sensing domain, or pore-forming domains as shown Fig. 6. Structural adjustments of this kind, in response to heme binding, would provide a mechanism for closure of the channel, because of the proximity of the N-terminal Cap domain to vital regulatory domains of channel gating (25). Relevant in this context is the observation that free heme affects channel function in the A-type potassium channels and, crucially, that the heme binds to the inactivation domain on the N-terminal region (30). We have no evidence for heme binding directly to the Cap domain in hERG3-eag, but changes in conformation of the N-terminal regions—induced either directly (by heme binding to N termini) or indirectly (by heme binding to adjacent domains, such as PAS)—might plausibly provide a mechanism for ion channel regulation.

Experimental procedures

Chemicals and reagents

All reagents were from Sigma–Aldrich unless otherwise stated. CO solutions were prepared by bubbling bath solution with CO gas. Iron protoporphyrin IX (hemin; Fig. S1*A*) was purchased from Sigma–Aldrich. Aqueous stock solutions of heme for all spectroscopic and electrophysiological experiments were prepared by dissolving solid heme in 0.1 M NaOH; final concentrations were calculated spectrophotometrically ($\epsilon_{385} = 58.4$ mM^{-1} cm^{-1} (44)) and diluted accordingly to 500 nM prior to use.
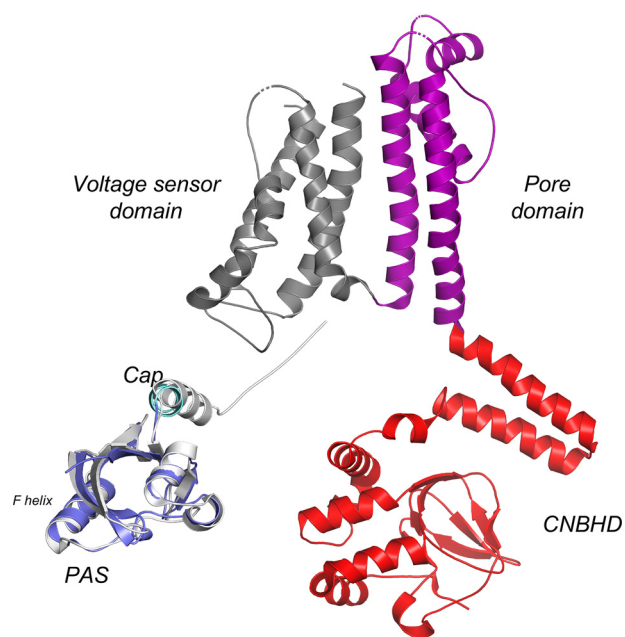

Figure 6. Cryo-EM structure of the hERG1 (Kv11.1) channel (Protein Data Bank 5VA1), showing the CNBHD (*red*), the pore domain (*magenta*), and the voltage-sensing domain (*dark gray*). For direct comparison, the color schemes used for the CNBHD, pore, and voltage-sensing domains are the same as those shown schematically in Fig. 1. In addition, the PAS and Cap (in *light gray*) domains are also shown for hERG1, aligned with hERG3-eag crystal structure (PAS domain, in *purple*; Cap domain in light *blue*, color scheme as Fig. 1). Movements of the F-helix (labeled) or the Cap domain, induced by heme binding, might conceivably affect the conformations of the nearby CNBDH, pore, and voltage-sensing domains, which could provide a mechanism for channel regulation. Refer also to Fig. 1, which shows a schematic of the locations of each domain in relation to the overall channel structure. We have drawn cartoon schematics of heme-dependent regulation of several different ion channels previously (K_{ATP}, Slo1 (BK) and Kv1.4 channels (36)), and we envisage a similar mechanism of control here.

Heme–agarose affinity purification and MS of neuronal lysates

Neuronal lysates were screened for possible heme-binding proteins using a modification of a previously published heme–agarose affinity (45). Binding of target proteins to heme–agarose was performed as previously (46), with modifications (Fig. S1*B*) that minimize pulling down proteins that bind to the heme–agarose resin nonspecifically. Full details are given in the supporting information. Using this approach, only proteins that were displaced from the agarose beads to bind specifically to the (heme) competitor (*i.e.* more likely to be *bona fide* heme-binding proteins) were identified and subjected to proteomics analysis (Fig. S1*C*). The data are available via ProteomeXchange with identifier PXD019887.

Expression and purification of hERG3-eag domain

The human KCNH7 clone (imaGenes Gmbh, Berlin, Germany) was used to obtain a sequence encoding residues 1–135 of the N terminus of the human hERG3 channel, which comprises the Cap (residues 1–26) and PAS (residues 27–135) domains (Fig. 1 and Fig. S2*A*). We refer to the fragment encoding residues 1–135 as hERG3-eag. The hERG3-eag domain was expressed as an N-terminal His$_6$/S-tagged fusion protein in *E. coli* BL21(DE3) cells using a pLEICS-93 (PROTEX facility,

University of Leicester) expression vector. Cell cultures in LB media were grown at 37 °C containing ampicillin (0.1%) to an A_{600} of 0.6–0.7, at which point the temperature was reduced to 18 °C and isopropyl β-D-thiogalactoside (0.2 mM) was added. After overnight incubation, the cells were harvested, suspended in lysis buffer (50 mM phosphate, 100 mM NaCl, pH 7.00, 10% glycerol, 0.1% Triton, 0.1 M MgSO$_4$, 1 complete ULTRA Tablet Mini EASY pack (Roche), 1 mg/ml lysozyme, and 1 mg/ml DNase), lysed by sonication, and centrifuged to remove cell debris. The cell lysates were loaded onto a 5-ml Ni^{2+}–nitrilotriacetic acid (Qiagen) affinity column equilibrated with 50 mM phosphate, 100 mM NaCl, pH 7.00, 10% (v/v) glycerol, and 15 mM imidazole. After washing with equilibration buffer, the His$_6$/S-tagged proteins were eluted with 50 mM phosphate, 100 mM NaCl, pH 7.0, 10% glycerol, and 100 mM EDTA. The His$_6$/S tag was cleaved with a His-tagged TEV-protease during overnight dialysis. The His$_6$/S tag and His-tagged TEV protease were removed by reverse Ni^{2+}–nitrilotriacetic acid affinity column, and the proteins were purified to homogeneity with size-exclusion chromatography (Superdex 200, GE Healthcare) using 50 mM phosphate, 100 mM NaCl, pH 7.0 (Fig. S2*B*). Protein concentrations were determined using a Bradford assay.

Optical absorption spectroscopy

Absorption spectra (25.0 °C) were obtained using a double beam spectrophotometer (PerkinElmer Lambda 40) or a Kontron Uvikon UV-visible spectrometer. Ferric heme-bound hERG3-eag was obtained by the addition of heme to hERG3-eag in 50 mM HEPES, 50 mM NaCl, pH 7.5. The reduced protein was obtained by anaeorobic addition of dithionite, and the ferrous-CO complex by gentle bubbling of CO through the reduced protein. Values of K_d for binding of ligands (heme, CO) to hERG3 (3–5 mM) were obtained at 25.0 °C in 50 mM HEPES, 50 mM NaCl, pH 7.5, as described previously (12). Heme dissociation was measured by reacting the ferric heme–hERG3-eag complex (6.4 μM) with a 5.6-fold excess of apomyoglobin (36 μM); the reaction was followed at 408 nm (50 mM HEPES, 50 mM NaCl, pH 7.5).

Resonance Raman spectroscopy

Samples (50 μl, in 50 mM HEPES, 50 mM NaCl, pH 7.5) of ferric heme and its complexes were prepared in quartz EPR tubes and placed in a homemade spinning cell, at room temperature, to avoid local heating and to prevent photodissociation and degradation. Protein concentrations were in the range 90–120 μM, and substoichiometric concentrations of heme (to 0.8 equivalents) were added to the protein to ensure that no excess of heme was present. Raman excitation at 413.1 nm was achieved with a laser power <10 mW from an Innova 90 Kr$^+$ laser (Coherent, Palo Alto, CA, USA). Resonance Raman spectra were recorded using a two-stage monochromator (U1000, Jobin Yvon, Longjumeau, France) equipped with a front illuminated, deep-depleted CCD detector (Jobin Yvon, Longjumeau, France). Spectra correspond to an average of three different 1-h accumulations. The spectral accuracy was estimated to be $\pm$1 cm^{-1}. Baseline correction was performed using GRAMS 32 (Galactic Industries, Salem, NH) and Origin$^\circledR$. Sample integrity

was verified by following resonance Raman spectral evolution during the experiment.

EPR spectroscopy

EPR spectra were recorded on an Elexsys 500 X-band spectrometer (Bruker) equipped with a continuous-flow ESR 900 cryostat and an ITC504 temperature controller (Oxford Instruments, Abingdon, UK). Simulations were performed by using the Easyspin software package (47) and routines written in the Dorlet laboratory. Samples (100 μl, 100 μM total heme concentration, 4–5-fold excess protein) of the ferric heme complexes of hERG3-eag were prepared in 50 mM HEPES and 50 mM NaCl, pH 7.5, and transferred to quartz EPR tubes.

Electrophysiology

hERG3 currents were expressed in Chinese hamster ovary cells and currents were recorded using either whole-cell or macropatch (inside-out or cell attached) configurations of the patch clamp technique. hERG3 currents were recorded with an Axopatch 200 voltage clamp amplifier, digitized using a Digidata 1440A interface, and acquired and analyzed using pClamp 10.3 software (Molecular Devices, Sunnyvale, CA, USA). For whole cell recordings the intracellular solution contained 30 mM KOH, 110 mM KCl, 1.2 mM MgCl$_2$, 1 mM CaCl$_2$, 10 mM EGTA, 5 mM HEPES, 1 mM ATP, titrated to pH 7.2 with KOH. The cells were superfused with normal bath solution containing 135 mM NaCl, 10 mM KCl, 5 mM glucose, 2 mM MgCl$_2$, 2 mM CaCl$_2$ and 10 mM HEPES, titrated to pH 7.3 with NaOH. Macropatch currents were recorded in equimolar K$^+$ solutions. The bath solution contained 40mM KOH, 80 mM KCl, 10 mM K$_2$SO$_4$, 10 mM HEPES, 5 mM EGTA, 5 mM HEDTA, and 10 glucose, pH 7.2. Pipette solution contained 140 mM KCl, 1 mM MgCl$_2$, 0.1 mM CaCl$_2$, and 10 mM HEPES, pH 7.4. To prevent rapid and complete current rundown, 10 μM phosphatidylinositol 4,5-bisphosphate was added to the bath solution in all excised inside-out macropatch recordings.

Aqueous stock solutions of ferric heme for electrophysiology experiments were prepared by dissolving heme in 0.1 M aqueous NaOH and mixing for 10 min, followed by centrifugation at 4,000 × g for 10 min and dilution as required. Final solutions contained 1 mM reduced GSH. Aliquots of heme were made fresh daily. All experiments were conducted at room temperature (22 $\pm$ 1 °C). The data are presented as means $\pm$ S.E. of n experiments.

Crystallization and data collection

A crystal of hERG3-eag (amino acids 1–135) was grown using sitting-drop vapor diffusion at 295 K. The crystallization drop was set up by mixing hERG3-eag (15 mg/ml, in 50 mM NaCl, 1 mM tris(2-carboxyethyl)phosphine) in a 1:1 ratio with reservoir solution (0.1 M NaCl, 0.1 M HEPES, pH 7.5, 1.6 M (NH$_4$)$_2$SO$_4$). A transparent crystal appeared after 4 weeks. The crystal was prepared for X-ray diffraction by brief immersion in the reservoir solution containing 25% glycerol for cryo-protection followed by flash vitrification in liquid nitrogen. X-ray diffraction data were collected at Diamond Light Source on Beamline I03. 3600 images of 0.05 degree were collected with an

exposure time of 0.039 s/image using 0.976 Å radiation. The crystal belongs to the space group P4$_3$2$_1$2 with unit cell dimensions $a = b = 32.78$ Å, $c = 200.68$ Å, $\alpha = \beta = \gamma = 90°$ (Table S2). The data were processed and scaled with DIALS software from the CCP4 program suite (48). The structure was determined by molecular replacement in PHASER (49) using the hERG1 PAS domain (Protein Data Bank code 4HQA (50)) as the search model and refined with REFMAC5 (51). The model was refined to a resolution of 1.39 Å with R_{work} and R_{free} values of 18.2 and 23.4%, respectively. The final cycles of refinement included extrapolated hydrogen atoms with anisotropic atomic displacement parameters (B) for all atoms. Data collection and refinement statistics are in Table S2 (Protein Data Bank code 6Y7Q), and the weighting scheme is given in Table S3.

MS analysis was carried out on a hERG3-eag crystal. The crystal was dissolved in 50 mM HEPES, 50 mM NaCl, pH 7.5, and LC–MS was carried out using an RSLCnano HPLC system (Thermo Scientific) and an LTQ-Orbitrap-Velos mass spectrometer (Thermo Scientific). Samples were loaded at 0.1 ml/min onto a Vydac C8 5 μM 250-mm $\times$ 1-mm inner-diameter reverse-phase column (Grace Davison). The protein was desalted for 10 min in the loading buffer (0.1% formic acid) before elution using a 10-min linear gradient from 3 to 96% B (80% acetonitrile, 0.1% formic acid). The output of the column was sprayed directly into the H-ESI2 electrospray ion source of the mass spectrometer maintained at 5 kV. The FT analyzer was set to acquire 10 microscans over the m/z range 800–2000 Da in positive ion mode. The maximum injection time for MS was 150 ms, and the AGC target setting was 3e[6]. Protein charge-state distributions were deconvoluted using the Xtract function of the Xcalibur program (version 2.1.0.1139, Thermo Scientific).

Data availability

The atomic coordinates and diffraction data have been deposited in the Protein Data Bank (accession code 6Y7Q). The proteomics data are available via ProteomeXchange with identifier PXD019887. All other data are included in the article or are available on request from the corresponding author.

Conflict of interest—The authors declare that they have no conflicts of interest with the contents of this article.

Abbreviations—The abbreviations used are: PAS, Per–ARNT–Sim; hERG3-eag, residues 1–135 of the N terminus of the human hERG3 channel, comprising the Cap and PAS domains; 5c-HS, ferric five-coordinate high-spin complex; CNBHD, cyclic nucleotide-binding homology domain.

References

1. Taylor, B. L., and Zhulin, I. B. (1999) PAS domains: internal sensors of oxygen, redox potential, and light. *Microbiol. Mol. Rev.* **63,** 479–506 CrossRef Medline
2. Henry, J. T., and Crosson, S. (2011) Ligand-binding PAS domains in a genomic, cellular, and structural context. *Annu. Rev. Microbiol.* **65,** 261–286 CrossRef Medline
3. Möglich, A., Ayers, R. A., and Moffat, K. (2009) Structure and signaling mechanism of Per–ARNT–Sim domains. *Structure* **17,** 1282–1294 CrossRef Medline
4. Shimizu, T., Lengalova, A., Martínek, V., and Martínková, M. (2019) Heme: emergent roles of heme in signal transduction, functional regulation and as catalytic centres. *Chem. Soc. Rev.* **48,** 5624–5657 CrossRef Medline
5. Shimizu, T., Huang, D., Yan, F., Stranava, M., Bartosova, M., Fojtíková, V., and Martínková, M. (2015) Gaseous O$_2$, NO, and CO in signal transduction: structure and function relationships of heme-based gas sensors and heme-redox sensors. *Chem. Rev.* **115,** 6491–6533 CrossRef Medline
6. Freeman, S. L., Kwon, H., Portolano, N., Parkin, G., Venkatraman Girija, U., Basran, J., Fielding, A. J., Fairall, L., Svistunenko, D. A., Moody, P. C. E., Schwabe, J. W. R., Kyriacou, C. P., and Raven, E. L. (2019) Heme binding to human CLOCK affects interactions with the E-box. *Proc. Natl. Acad. Sci. U.S.A.* **116,** 19911–19916 CrossRef Medline
7. Morais Cabral, J. H., Lee, A., Cohen, S. L., Chait, B. T., Li, M., and Mackinnon, R. (1998) Crystal structure and functional analysis of the HERG potassium channel N terminus: a eukaryotic PAS domain. *Cell* **95,** 649–655 CrossRef Medline
8. Smith, A. T., Pazicni, S., Marvin, K. A., Stevens, D. J., Paulsen, K. M., and Burstyn, J. N. (2015) Functional divergence of heme-thiolate proteins: a classification based on spectroscopic attributes. *Chem. Rev.* **115,** 2532–2558 CrossRef Medline
9. Reynolds, M. F., Shelver, D., Kerby, R. L., Parks, R. B., Roberts, G. P., and Burstyn, J. N. (1998) EPR and electronic absorption spectroscopies of the CO-sensing CooA protein reveal a cysteine-ligated low-spin ferric heme. *J. Am. Chem. Soc.* **35,** 9080–9081 CrossRef
10. Pazicni, S., Lukat-Rodgers, G. S., Oliveriusová, J., Rees, K. A., Parks, R. B., Clark, R. W., Rodgers, K. R., Kraus, J. P., and Burstyn, J. N. (2004) The redox behavior of the heme in cystathionine β-synthase is sensitive to pH. *Biochemistry* **43,** 14684–14695 CrossRef Medline
11. Hargrove, M. S., Singleton, E. W., Quillin, M. L., Ortiz, L. A., Phillips, G. N., Jr., Olson, J. S., and Mathews, A. J. (1982) His[64](E7)-Tyr apomyoglobin as a reagent for measuring rates of hemin dissociation. *J. Biol. Chem.* **269,** 4207–4214 Medline
12. Kapetanaki, S. M., Burton, M. J., Basran, J., Uragami, C., Moody, P. C. E., Mitcheson, J. S., Schmid, R., Davies, N. W., Dorlet, P., Vos, M. H., Storey, N. M., and Raven, E. (2018) A mechanism for CO regulation of ion channels. *Nat. Commun.* **9,** 907 CrossRef Medline
13. Kalsbeck, W. A., Robertson, D. E., Pandey, R. K., Smith, K. M., Dutton, P. L., and Bocian, D. F. (1996) Structural and electronic properties of the

heme cofactors in a multi-heme synthetic cytochrome. *Biochemistry* **35,** 3429–3438 CrossRef Medline

14. Kitanishi, K., Igarashi, J., Hayasaka, K., Hikage, N., Saiful, I., Yamauchi, S., Uchida, T., Ishimori, K., and Shimizu, T. (2008) Heme-binding characteristics of the isolated PAS: a domain of mouse Per2, a transcriptional regulatory factor associated with circadian rhythms. *Biochemistry* **47,** 6157–6168 CrossRef Medline

15. Stone, J. R., Sands, R. H., Dunham, W. R., and Marletta, M. A. (1995) Electron paramagnetic resonance spectral evidence for the formation of a pentacoordinate nitrosyl–heme complex on soluble guanylate cyclase. *Biochem. Biophys. Res. Commun.* **207,** 572–577 CrossRef Medline

16. Stone, J. R., and Marletta, M. A. (1994) Soluble guanylate cyclase from bovine lung: activation with nitric oxide and carbon monoxide and spectral characterization of the ferrous and ferric states. *Biochemistry* **33,** 5636–5640 CrossRef Medline

17. Gupta, N., and Ragsdale, S. W. (2011) Thiol-disulfide redox dependence of heme binding and heme ligand switching in nuclear hormone receptor rev-erbβ. *J. Biol. Chem.* **286,** 4392–4403 CrossRef Medline

18. Yi, L., Jenkins, P. M., Leichert, L. I., Jakob, U., Martens, J. R., and Ragsdale, S. W. (2009) Heme regulatory motifs in heme oxygenase-2 form a thiol/disulfide redox switch that responds to the cellular redox state. *J. Biol. Chem.* **284,** 20556–20561 CrossRef Medline

19. Yi, L., Morgan, J. T., and Ragsdale, S. W. (2010) Identification of a thiol/disulfide redox switch in the human BK channel that controls its affinity for heme and CO. *J. Biol. Chem.* **285,** 20117–20127 CrossRef Medline

20. Yi, L., and Ragsdale, S. W. (2007) Evidence that the heme regulatory motifs in heme oxygenase-2 serve as a thiol/disulfide redox switch regulating heme binding. *J. Biol. Chem.* **282,** 21056–21067 CrossRef Medline

21. Light, W. R., 3rd,., and Olson, J. S. (1990) Transmembrane movement of heme. *J. Biol. Chem.* **265,** 15623–15631 Medline

22. Asher, V., Sowter, H., Shaw, R., Bali, A., and Khan, R. (2010) Eag and HERG potassium channels as novel therapeutic targets in cancer. *World J. Surg. Oncol.* **8,** 113 CrossRef Medline

23. Ganetzky, B., Robertson, G. A., Wilson, G. F., Trudeau, M. C., and Titus, S. A. (1999) The eag family of K⁺ channels in *Drosophila* and mammals. *Ann. N.Y. Acad. Sci.* **868,** 356–369 CrossRef Medline

24. Whicher, J. R., and MacKinnon, R. (2016) Structure of the voltage-gated K⁺ channel Eag1 reveals an alternative voltage sensing mechanism. *Science* **353,** 664–669 CrossRef Medline

25. Wang, W., and MacKinnon, R. (2017) Cryo-EM structure of the open human ether-a-go-go–related K⁺ channel hERG. *Cell* **169,** 422–430e410 CrossRef Medline

26. Lörinczi, E., Helliwell, M., Finch, A., Stansfeld, P. J., Davies, N. W., Mahaut-Smith, M., Muskett, F. W., and Mitcheson, J. S. (2016) Calmodulin regulates human ether a Go-Go 1 (hEAG1) potassium channels through interactions of the Eag domain with the cyclic nucleotide binding homology domain. *J. Biol. Chem.* **291,** 17907–17918 CrossRef Medline

27. Muskett, F. W., Thouta, S., Thomson, S. J., Bowen, A., Stansfeld, P. J., and Mitcheson, J. S. (2011) Mechanistic insight into human ether-a-go-go–related gene (hERG) K⁺ channel deactivation gating from the solution structure of the EAG domain. *J. Biol. Chem.* **286,** 6184–6191 CrossRef Medline

28. Chen, J., Zou, A., Splawski, I., Keating, M. T., and Sanguinetti, M. C. (1999) Long QT syndrome-associated mutations in the Per–ARNT–Sim (PAS) domain of HERG potassium channels accelerate channel deactivation. *J. Biol. Chem.* **274,** 10113–10118 CrossRef Medline

29. Gianulis, E. C., Liu, Q., and Trudeau, M. C. (2013) Direct interaction of eag domains and cyclic nucleotide-binding homology domains regulate deactivation gating in hERG channels. *J. Gen. Physiol.* **142,** 351–366 CrossRef Medline

30. Sahoo, N., Goradia, N., Ohlenschlager, O., Schonherr, R., Friedrich, M., Plass, W., Kappl, R., Hoshi, T., and Heinemann, S. H. (2013) Heme impairs the ball-and-chain inactivation of potassium channels. *Proc. Natl. Acad. Sci. U.S.A.* **110,** E4036–E4044 CrossRef Medline

31. Tang, X. D., Xu, R., Reynolds, M. F., Garcia, M. L., Heinemann, S. H., and Hoshi, T. (2003) Haem can bind to and inhibit mammalian calcium-dependent Slo1 BK channels. *Nature* **425,** 531–535 CrossRef Medline

32. Jaggar, J. H., Li, A., Parfenova, H., Liu, J., Umstot, E. S., Dopico, A. M., and Leffler, C. W. (2005) Heme is a carbon monoxide receptor for large-conductance Ca²⁺-activated K⁺ channels. *Circ. Res.* **97,** 805–812 CrossRef Medline

33. Burton, M. J., Kapetanaki, S. M., Chernova, T., Jamieson, A. G., Dorlet, P., Santolini, J., Moody, P. C. E., Mitcheson, J. S., Davies, N. W., Schmid, R., Raven, E. L., and Storey, N. M. (2016) A heme-binding domain controls regulation of ATP-dependent potassium channels. *Proc. Natl. Acad. Sci. U.S.A.* **113,** 3785–3790 CrossRef Medline

34. Augustynek, B., Kudin, A. P., Bednarczyk, P., Szewczyk, A., and Kunz, W. S. (2014) Hemin inhibits the large conductance potassium channel in brain mitochondria: a putative novel mechanism of neurodegeneration. *Exp. Neurol.* **257,** 70–75 CrossRef Medline

35. Wang, S., Publicover, S., and Gu, Y. (2009) An oxygen-sensitive mechanism in regulation of epithelial sodium channel. *Proc. Natl. Acad. Sci. U.S.A.* **106,** 2957–2962 CrossRef Medline

36. Wu, J. Y., Qu, H. Y., Shang, Z. L., Tao, S. T., Xu, G. H., Wu, J., Wu, H. Q., and Zhang, S. L. (2011) Reciprocal regulation of Ca²⁺-activated outward K⁺ channels of *Pyrus pyrifolia* pollen by heme and carbon monoxide. *New Phytol.* **189,** 1060–1068 CrossRef Medline

37. Smith, A. G., Raven, E. L., and Chernova, T. (2011) The regulatory role of heme in neurons. *Metallomics* **3,** 955–962 CrossRef Medline

38. Li, Z. (2011) *Heme Biology: The Secret Life of Heme in Regulating Diverse Biological Processes*, World Scientific, Singapore

39. Robinson, S. R., Dang, T. N., Dringen, R., and Bishop, G. M. (2009) Hemin toxicity: a preventable source of brain damage following hemorrhagic stroke. *Redox Rep.* **14,** 228–235 CrossRef Medline

40. Kurokawa, H., Lee, D. S., Watanabe, M., Sagami, I., Mikami, B., Raman, C. S., and Shimizu, T. (2004) A redox-controlled molecular switch revealed by the crystal structure of a bacterial heme PAS sensor. *J. Biol. Chem.* **279,** 20186–20193 CrossRef Medline

41. Gong, W., Hao, B., and Chan, M. K. (2000) New mechanistic insights from structural studies of the oxygen-sensing domain of *Bradyrhizobium japonicum* FixL. *Biochemistry* **39,** 3955–3962 CrossRef Medline

42. Ng, C. A., Hunter, M. J., Perry, M. D., Mobli, M., Ke, Y., Kuchel, P. W., King, G. F., Stock, D., and Vandenberg, J. I. (2011) The N-terminal tail of hERG contains an amphipathic α-helix that regulates channel deactivation. *PLoS One* **6,** e16191 CrossRef Medline

43. Wang, J., Myers, C. D., and Robertson, G. A. (2000) Dynamic control of deactivation gating by a soluble amino-terminal domain in HERG K⁺ channels. *J. Gen. Physiol.* **115,** 749–758 CrossRef Medline

44. Dawson, R. M. C., Elliot, D. C., Elliot, W. H., and Jones, K. M. (1975) *Data for Biochemical Research*, Oxford University Press, Oxford, UK

45. Otto, B. R., van Dooren, S. J., Nuijens, J. H., Luirink, J., and Oudega, B. (1998) Characterization of a hemoglobin protease secreted by the pathogenic *Escherichia coli* strain EB1. *J. Exp. Med.* **188,** 1091–1103 CrossRef Medline

46. Lee, B. G. (1992) Isolation of an outer membrane hemin-binding protein of *Haemophilus influenzae* type B. *Infect. Immun.* **60,** 810–816 CrossRef Medline

47. Stoll, S., and Schweiger, A. (2006) EasySpin, a comprehensive software package for spectral simulation and analysis in EPR. *J. Magn. Reson.* **178,** 42–55 CrossRef Medline

48. Collaborative Computational Project, Number 4 (1994) The CCP4 suite: programs for protein crystallography. *Acta Crystallogr. D Biol. Crystallogr.* **50,** 760–763 CrossRef Medline

49. McCoy, A. J., Grosse-Kunstleve, R. W., Adams, P. D., Winn, M. D., Storoni, L. C., and Read, R. J. (2007) Phaser crystallographic software. *J. Appl. Crystallogr.* **40,** 658–674 CrossRef Medline

50. Adaixo, R., Harley, C. A., Castro-Rodrigues, A. F., and Morais-Cabral, J. H. (2013) Structural properties of PAS domains from the KCNH potassium channels. *PLoS One* **8,** e59265 CrossRef Medline

51. Murshudov, G. N., Vagin, A. A., and Dodson, E. J. (1997) Refinement of macromolecular structures by the maximum-likelihood method. *Acta Crystallogr.* **53,** 240–255 CrossRef Medline